A V Chankin
G Saibene

Interpretation of the H-mode Operational Diagram through Similarity Parameters for Edge Transport Mechanisms

Interpretation of the H-mode Operational Diagram through Similarity Parameters for Edge Transport Mechanisms

A V Chankin, G Saibene.

JET Joint Undertaking, Abingdon, Oxfordshire, OX14 3EA,

ABSTRACT

ELMy H-modes are currently the main scenario envisaged for ITER operation. The reliable extrapolation of present experimental data to ITER requires a model which is capable of explaining the variety of experimental phenomena observed in high density H-modes. In particular, it has to provide correct scalings for the main operational points identified on the edge n_e-T_e operational diagram. In all tokamaks, the maximum density was found to scale approximately as $\bar{n}_e \sim B/qR$ in agreement with the Greenwald/Hugill scaling. The present paper is an attempt to construct such a model with the assumption that behaviour of high density ELMy H-modes can be explained through the similarity of edge transport mechanisms.

Three dimensionless parameters have been identified as the most representative for the high density H-mode operation: a) $F_\beta = q^2 R \nabla\beta / f(s)$ representing the ideal ballooning limit, b) collisionality $\nu_e^* = Z_{eff} nqR / T_e^2$ which is postulated to be responsible for the transition from type I to type III ELMs and c) the L-H transition boundary represented by $F_{L-H} = T_e^3 / (B^2 L_\perp Z_{eff} / \sqrt{m_i})$. Fixing any two out of these three parameters allows one to find scalings for the main operational points in the edge n_e-T_e diagram and reproduce the Greenwald/Hugill dependencies.

More detailed scalings for the type I to type III ELM transition point, which may be of particular interest for a reactor, show that the critical edge density should scale as $n_e \sim B^\alpha / q^\beta R^\gamma$, where $\alpha \approx 1$, $\beta > 1$ and $\gamma < 1$ (but being close to unity). One particular scaling for the critical edge density (near or at the separatrix) consistent with the collisional skin-depth model was found to be in a good agreement with results of a dedicated series of experiments on JET which confirmed the $\bar{n}_e \sim B/q^{5/4}$ dependence for the line average density. The scaling for $n_{e,crit}$, however, was found to be not very sensitive to the transport model selected and other models yielded very similar dependencies.

1. INTRODUCTION

A fusion reactor has to satisfy stringent criteria for high fusion yield (implying both high plasma density and energy confinement, but below the critical β) and at the same time provide favourable conditions for power exhaust to the plasma facing surfaces. In the regime of improved confinement (H-mode) [1] which is presently the main scenario for the ITER prototype reactor, these two conditions may come into conflict with each other, as it will be shown in section 2 of this paper. In fact, the standard ITER scenario for ignition [2] requires a confinement enhancement factor H of 1 (according to the ITER97-EPS scaling [3]) at a plasma density of about 1×10^{20} m^{-3} in steady state. In existing experiments ([4], [5], [6], [7], [8] and [9]) good energy confinement is normally obtained only at plasma densities that extrapolate to values that are

insufficient for ignition. Steady state H-mode conditions are obtained in present day experiments either with type I or type III Edge Localised Modes (ELMs) (for the definition of ELM types we refer to the review articles [10] and [11]). The type I ELMs occur near the ideal ballooning limit and are believed by some authors to originate from ideal ballooning instabilities caused by the sharp pressure gradients at the edge, characteristic of the H-mode regime (see e.g. a review of models for ELMs in [12]). Each ELM is accompanied by a sudden expulsion of energy and particles from the confined plasma. Extrapolation of the power load to plasma facing components measured in present day machines [13] indicates that the resulting erosion would be unacceptable for a reactor. As the plasma density is increased by gas fuelling, the ELM frequency increases and their amplitude decreases and, finally, at high densities type I ELMs are replaced by high frequency, small amplitude type III ELMs. This change in the ELM character is generally accompanied by a degradation of the energy confinement. The predominant point of view is that type III ELMs are caused by resistive ballooning instabilities at the plasma edge [12].

Experimentally, it is found that a good measure for the density to be considered "high" or "low" is the fraction of the density with respect to the Greenwald density limit (GDL), $\bar{n}_e \equiv n_{GW}[m^{-3}] = 10^{14} \frac{I_p[A]}{\pi a^2[m^2]}$ [14], where $\bar{n}_e$ is the line averaged density, I_p is the plasma current and a is the plasma minor radius. For fixed plasma elongation, the functional dependence of this density can also be written in the form of the Hugill density limit: $\bar{n}_e \sim B/qR$ [15], which gives $\bar{n}_e \sim j$ (j is the current density). This functional dependence is used in the remainder of the paper, while the numerical values for the analysis of the experimental data are calculated from the GDL expression. The Greenwald/Hugill expressions for the maximum density were obtained from multi-machine scaling of Ohmic and L-mode density limit data. It is therefore interesting to note that this limit, or very similar expressions (of the form $B^\alpha/q^\beta R^\gamma$ with coefficients α, β and γ close to unity) do indeed represent very well the maximum density achievable in H-mode discharges. In the present paper we first give a summary of experimental observations related to operation at high densities in ELMy H-modes. We then provide a physics basis for these observations through analysis of the similarity parameters for the main edge transport mechanisms. By fixing pairs of similarity parameters corresponding to various characteristic points on the edge n_e-T_e operational diagram, scalings for n_e and T_e can be obtained. The scalings for the density are indeed of the form $B^\alpha/q^\beta R^\gamma$, indicating that this combination is an important similarity parameter for edge physics. These scalings may be useful in projecting critical edge parameters to future machines.

2. SUMMARY OF EXPERIMENTAL OBSERVATIONS WITH THE MARK II DIVERTOR

The recent experimental campaign in JET has provided valuable information on the study of high density ELMy H-modes. Its results were reported in [4], [16], [17], [18] and [19]. Series of plasma discharges were carried out for a given plasma magnetic geometry (shape, edge shear, divertor magnetic flux expansion and separatrix strike point location), with a fixed level of Neutral Beam (NB) power injection. The length of the heated phase was sufficient to allow the main plasma parameters to reach steady state compared to the energy confinement time τ_E (in general t>$4\tau_E$). The same discharge was repeated with increasing levels of constant gas fuelling.
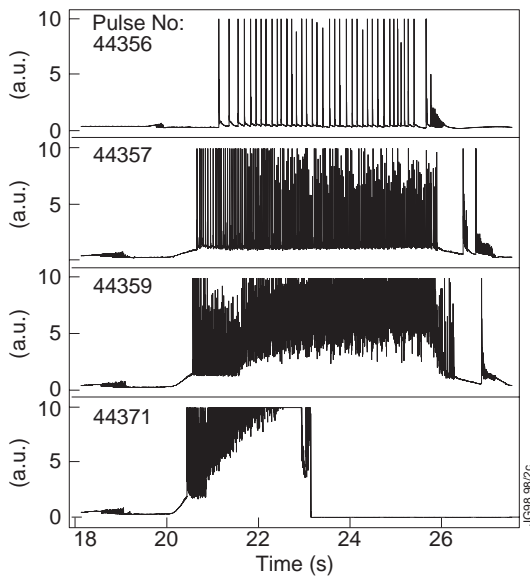

Figure 1: Time traces of divertor D_a emission for the JET plasma discharges 44356, 44357, 44359 and 44371 (2.6MA/2.7T, 12MW NBI input power in Deuterium). For this experiment, the constant gas fuelling rate was increased from 0 (#44356) to ~$4x10^{22}s^{-1}$ (#44371). The plasma average density correspondingly increased from ~$7x10^{19}m^{-3}$ to ~$9x10^{19}m^{-3}$ (95% of the GDL for this plasma configuration, while the plasma stored energy decreased from ~6MJ to ~4MJ at the highest gas rate.

It is a general observation for this type of experiments that the increase of the plasma density caused by the external gas fuelling is accompanied by the decrease of the global energy confinement. For the particular experiment illustrated in Figure 1, the maximum density achieved while maintaining H-mode confinement (albeit strongly degraded) is just below the GDL. As the density is raised, the ELM frequency increases and clusters of smaller and more frequent ELMs begin to occur, in particular after a type I ELM, and become more frequent until they dominate the ELM behaviour of the discharge. We identify these as type III ELMs, according to the standard criterion of ELMs classification (frequency of the ELMs inversely proportional to the input power [10]).

This change in the character of the ELMs is coincident with the deterioration of the global energy confinement (typically H97 decreases from near 0.9 down to ~0.6, Figure 2).

The plasma density does not always saturate at the transition from type I to III ELMs, and may reach its maximum during the type III phase. Eventually, when the plasma is still in H-mode, albeit at a reduced confinement (with $H_{97}<1$), and in spite of the continuous fuelling, the density first saturates and then decreases. If the fuelling is maintained, the plasma eventually reverts to L-mode with no ELMs present.

Saibene et al. [4] have proposed an interpretation of the "density limit" in ELMy H-modes as a transport phenomenon, correlating the reduced effective particle confinement to the changes
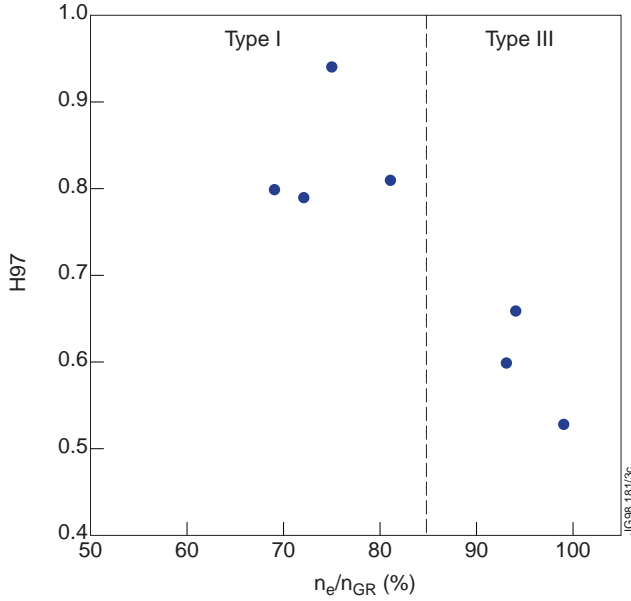
3

Figure 2: Global energy confinement as function of the plasma line average density normalised to the Greenwald density limit, for the same plasma discharges as in Figure 1.

in the global energy confinement as follows: increased transport at the edge of the plasma (i.e. reduced local confinement) clamps the density below a certain limit despite an increase in the external fuelling. TRANSP code simulations of these degraded confinement, high density discharges indeed show that the reduction in the global energy confinement corresponds to enhanced losses in the outer 25% of the plasma radius, whilst the central thermal conductivities are not affected, compared to an unfuelled case. These results indicate that the properties of the plasma near the edge of the pedestal of temperature and density profiles, characteristic of the H-mode (providing the boundary conditions for the core plasma) may be crucial in explaining the global plasma properties of ELMy H-modes at high densities. The results obtained in JET are consistent with observations reported from other tokamaks. In ASDEX-Upgrade [6], plasmas displaying type III ELMs were obtained at densities near the GDL. The confinement of these plasmas, however, was strongly degraded to values almost characteristic of L-mode, in spite of the ELM activity. DIII-D [8] reports densities above the GDL, but again at the expense of the global energy confinement of the plasma, depressed to near L-mode values.

Borrass et al. [20] have developed a model that extends the treatment of L-mode density limits [21] to the case of H-modes. In this model, the onset of the H-mode density limit is related to plasma detachment at the divertor plates. Given the poor correlation observed experimentally in JET between plasma detachment at the divertor plates (between ELMs) [16] and the confinement degradation at high density, in this paper we take the view that detachment at high density is not responsible for the H-mode density limit.

The survey of the available experimental evidence shows that the maximum density achieved in steady state H-modes for Tokamaks of different sizes scales approximately as predicted by the Hugill-Greenwald dependencies, supporting these power-independent B/qR type of scalings . However, experimental results deviating from this simple dependence were reported previously from ASDEX [22], where an increase of the density limit over the GDL by as much as 30% was achieved by operating at low edge q, indicating that the dependence of the maximum density on the safety factor q is stronger than $1/q$. In that particular experiment, plasma densities above the GDL were achieved while maintaining good H-mode confinement by the

4

combination of high plasma current and low magnetic field. As we will show in Sections 5 and 7, these results can be deduced from the strong (quadratic) dependence of the ideal ballooning limit (at fixed B) on q.

3. THE EDGE N_E-T_E OPERATIONAL DIAGRAM

Further insight into the mechanisms determining the ELM behaviour and the density limit in ELMy H-modes is gained by analysing these discharges in terms of local edge plasma parameters [7]. The schematic diagram in Figure 3 identifies the range of edge parameters for H-mode operation, as being defined by the ideal ballooning limit boundary and a curve representing the critical temperature for the L-H transition.

Figure 3 shows an "idealised" representation of the evolution of the plasma edge pedestal n_e and T_e in a typical high density discharge with gas fuelling. After the application of additional heating and the L-H transition, the plasma enters an ELM-free H-mode period. This is characterised by an increase of the plasma stored energy and density, reflected locally by a fast increase of the edge T_e and a somewhat slower increase of the edge n_e. The ELM-free period terminates with the first type I ELM, triggered when the edge pressure (defined as the product of the edge n_e and T_e) reaches a critical value, associated with the ideal ballooning limit. During each ELM the edge T_e and n_e are reduced and subsequently recover until the critical edge pressure is reached. In steady state, the average plasma stored energy, temperature and density are constant, and the repetitive type I ELMs would be represented by a closed loop on the n_e-T_e diagram.
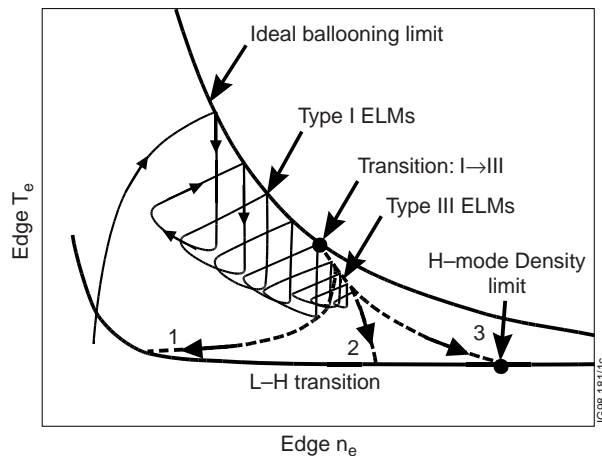

Figure 3: Schematic edge n_e-T_e diagram summarising the main features of an ELMy H-mode gas puffed discharge in terms of the plasma edge pedestal parameters.

Figure 3 represents a non-steady state case in which the addition of external fuelling causes the plasma density to increase. At the plasma edge, this corresponds to an increase in n_e and decrease of T_e, at constant edge pressure (gradient), but increasing edge collisionality. At some point, type I ELMs are replaced by type III ELMs (labelled as transition: I→III in Figure 3), and the maximum n_e and T_e at the ELM no longer follow the ideal ballooning curve. The exact trajectory of the type III ELMy phase in the edge n_e-T_e space will depend on the details of the particular experiment (the variation in gas puff rate, power input, impurity content etc. are likely to affect the evolution of the edge particle and energy content), and is schematically represented by

5

routes 1, 2 and 3 in Figure 3. Route 1 describes a simultaneous loss of energy and particle confinement shortly after the type I to III transition. Route 2 represents a trajectory where energy depletion dominates whereas particle content is unaffected. Finally, route 3 corresponds to an optimum scenario, of reduced energy and particle losses compared to 1 and 2, that allows one to reach the highest density in H-mode. For the first case, the maximum density in H-mode is reached before the H-L transition, whereas for the two other cases, the maximum density coincides with the transition to the L-mode. The experimental evidence from JET indicates that the H-mode density limit is achieved in most cases before the H-L transition, and that the edge parameters follow either route 1 or some other path between routes 1 and 2, while route 3 is less common.

4. THE MAIN DIMENSIONLESS PARAMETERS

Having summarised the main experimental observations, the authors are of the opinion that H-mode density limits in different machines are "similar" in the sense that they have similar experimental signatures and appear to be described by the functional dependence $\bar{n}_e \sim B^\alpha / q^\beta R^\gamma$ with coefficients α, β and γ close to unity. We are ignoring the possible effects of the plasma elongation, since very little experimental information has so far been obtained on this dependence, in particular for H-mode density limits. Furthermore, again in accordance with experimental observations (such as the possibility to raise the core density by deep pellet injection compared with the gas puff discharges as on ASDEX-Upgrade [6]), we will be assuming that it is the edge density which is limited in the ELMy H-modes rather than the core density. In accordance with experimental results from JET described earlier, we believe that the H-mode density limit reached near the plasma edge is essentially due to transport phenomena.

The above considerations allow us to formulate the H-mode density limit through similarity parameters which account for the main transport mechanisms near the plasma edge. According to this formulation, the H-mode density limit in different machines must be reached for certain values of the similarity parameters which are the same in all machines. The correct set of similarity parameters should account for both the edge transport due to ELMs and the periods in between ELMs. We will show that three parameters are sufficient to explain satisfactory the events on the n_e-T_e operational diagram in the approach to the H-mode density limit.

The first two parameters characterise the behaviour of ELMs which are, by definition, plasma edge phenomena. We will assume that the cause of type I ELMs is ultimately the gradient of plasma edge pressure. Assuming that type I ELMs are triggered at the ideal ballooning limit we have $\nabla\beta \sim f(s)/q^2 R$, and this limit can be expressed via the dimensionless parameter:

$$F_\beta = \frac{q^2 R \nabla\beta}{f(s)} \tag{1}$$

6

where β is the total plasma beta and $f(s)$ is a monotonically increasing function of the edge magnetic shear. Experimental evidence from JET [23] confirms the positive dependence of the critical edge pressure on magnetic shear. We note that the plasma edge of ELMy H-modes is characterised by high pressure gradients ∇p, and relatively low temperatures T_e (typically one third or less of the temperatures reached at the plasma edge in hot ion H-modes, [24] and [25]). These conditions at the edge should imply an increased role of ballooning effects due to the pressure gradient and a lesser role of kink modes, owing to a reduction of the edge current density due to the relatively low Ohmic contribution. Whether the ideal ballooning instability is indeed responsible for type I ELMs is, however, not absolutely clear at present ([17],[26]), but at least the fact that the functional dependence of the maximum edge pressure gradient is proportional to the square of the plasma current is well established experimentally [27].

In the case of type III ELMs, we will relate them with resistive ballooning instabilities. To account for the plasma edge resistivity, we include the collisionality as the second similarity parameter:

$$\nu_e^* = Z_{eff} n_e q R / T_e^2 \qquad (2)$$

In the following analysis we will assume that the combination of the two similarity parameters (1) and (2) describes the threshold for type III ELMs. The exact form of this threshold cannot be determined from the dimensional analysis alone. The working assumption is therefore that the onset of the type III ELMs (when moving from type I ELMy regime by increasing the plasma density, as illustrated schematically in Figure 3) is caused by increased collisionality.

Whereas the position of the sharp pressure gradients in H-mode plasmas can be identified experimentally, the exact location of the critical T_e is less certain. We argue that its location is in the "edge", i.e. between the top of the pedestal and the separatrix. We take the view that the extreme edge, near the separatrix, is most likely to be the critical position since this is where the boundary conditions for the whole plasma column are defined. The following analysis in this section, however, is local and does not depend on the particular position within this range.

The third similarity parameter is related to the confinement between ELMs. In accordance with the experimental observations (see e.g. Ref. [28] from JET) the threshold for the L-H transition depends mainly on the critical edge temperature T_e, which increases with the toroidal field. An expression for the L-H transition threshold which combines these main experimental features, has been proposed by Chankin and Matthews [29] based on the idea of the suppression of the electrostatic drift turbulence (at low plasma T_e and β) by the finite skin-depths (as the T_e and β are raised by the increased input power). The critical parameter for this suppression is the ratio of the ion Larmor radius $\rho_s = c\sqrt{m_i T_e} / eB$ to the collisional skin-depth Δ_{skin}, which yields the following scaling: $T_e^3 \sim B^2 L_\perp Z_{eff} / \sqrt{m_i}$ ($L_\perp$ being the perpendicular decay length for the density or, if the density profile is flat, for temperature). This condition should apply near the

7

separatrix, where the plasma electron temperature is low, and therefore the plasma is collisional (the collisional skin-depth was used in the derivations). In accordance with [29], the ratio ρ_s / Δ_{skin} also represents the degree of electro-magnetism of small-scale fluctuations, which are simply drift modes in the electrostatic limit. Thus, the above scaling should also be relevant to the state of plasma turbulence and confinement between ELMs. Therefore the third parameter should be related to this scaling:

$$F_{L-H} = T_e^3 /(B^2 L_\perp Z_{eff} / \sqrt{m_i}) \tag{3}$$

In Figure 3, the L-H transition threshold T_e increases at low n_e. This reflects the fact that at low densities the skin-depth is defined by the collisionless electron conductivity due to electron inertia, giving rise to the critical condition for β rather than T_e [29] (see also [30] which contains numerical examples).

Having introduced the three similarity parameters for the description of ELMy H-modes, we can now re-plot the edge operational space in terms of the ν_e^*-F_β parameters (Figure 4). The ideal ballooning limit is represented now by a horizontal line (F_β =*constant*). In order to draw the L-H transition boundary, however, some assumptions about the gradients of the pressure and the characteristic decay length $L_\perp$ in Eq. (3) have to be made. In the simplest case of $T_e \sim T_i$, constant gradients, shear etc., the F_{L-H} parameter, which can be expressed through ν_e^* and F_β as

Figure 4: Schematic edge diagram in ν_e^*-F_β dimensionless parameter space corresponding to the diagram in Figure 3.

$F_{L-H} \sim \dfrac{F_\beta}{\nu_e^*} \times \dfrac{\lambda_p}{qL_\perp} \times \dfrac{f(s)}{\sqrt{m_i}}$, will correspond to a straight line for the L-H transition threshold in

the ν_e^*-F_β space going through the origin. λ_p is the pressure decay length following from $\nabla\beta = 4\pi / B^2 \times p / \lambda_p$. At low densities, since the critical condition for the L-H transition is on β, the F_{L-H} parameter is represented by a segment of a horizontal line. Note that the assumption of the constant decay length $L_\perp$ has also been implicitly made by drawing the L-H transition as a horizontal line at medium to high densities in Figure 3.

5. GENERALISED FORM OF SCALINGS FOR H-MODE DENSITY LIMITS

Without having to describe the detailed mechanisms governing type III ELMs, and based only on the assumption that these ELMs are caused by resistive modes and that parameters (1) and
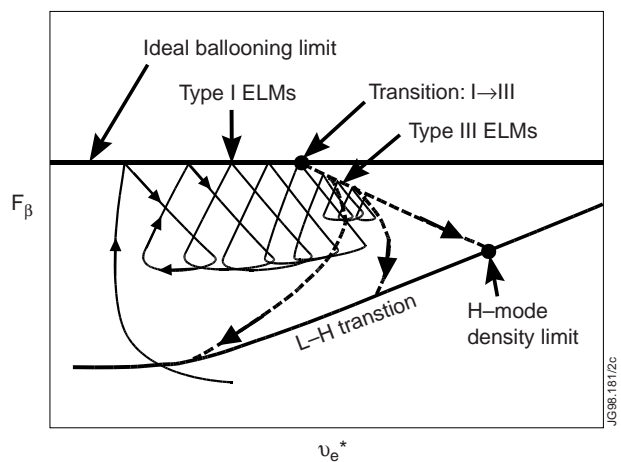
8

(2) adequately describe the source of both the ideal and resistive ballooning instabilities, one can derive a scaling law for the density which gives the boundary between type I and III ELMs. By fixing parameters (1) and (2) and eliminating the net temperature dependence, the following scaling for the critical density for the type I →III transition is obtained:

$$n_e(I \to III) \sim \frac{B^{4/3}}{q^{5/3}R}\lambda_p^{2/3}f(s)^{2/3} \times \left(\frac{T_e}{T_e + T_i}\right)^{2/3}\frac{1}{Z_{eff}^{1/3}} \tag{4}$$

where λ_p is the total pressure decay length. Note that the functional form of the threshold density has some similarity with the Hugill density limit ($n_e \sim B/qR$) for fixed shear, T_e/T_i ratio, λ_p and Z_{eff}. In this section we leave the pressure decay length as a free parameter. In Section 7 we derive more explicit scalings of $n_e(I \to III)$using different dependencies for λ_p corresponding to several transport models.

The second important issue for which a scaling can be easily obtained is the intersection point between the ideal ballooning limit curve and the L-H transition threshold boundary (outside the view on Figure 3). This intersection represents the maximum density that would be attained by a plasma that maintains type I ELMs while the edge density increases, until the edge temperature falls below the critical H-mode temperature. Fixing parameters (1) and (3), we obtain the following scaling for this density:

$$n_{e,max} \sim \frac{B^{4/3}}{q^2R}\frac{\lambda_p}{\lambda_\perp^{1/3}}f(s) \times \frac{T_e}{T_e + T_i}\frac{m_i^{1/6}}{Z_{eff}^{1/3}} \tag{5}$$

These two points anchor the whole high density space of the n_e - T_e operational diagram. The fact that the density (and hence, the temperature) scalings for these points are very close to each other, indicates that the shape of the high density operational space on this diagram is relatively independent of the machine/regime parameters and that it should be easily transferable from one machine to another to allow for a multi-machine scaling. Note that the close similarity between the scalings (4) and (5) has been achieved despite the original similarity parameters (2) and (3) having very different functional dependencies on physical parameters.

The derivation of the scaling for the density corresponding to the point marked "H-mode Density Limit" on Figure 3 is complicated by the fact that the "optimum" route 3 should be described in terms of all three parameters (1), (2) and (3). Unfortunately, we cannot determine the exact shape of this curve from dimensional considerations alone. Since the maximum density is somewhere in between the type I - type III ELM transition point and the marked "H-mode Density Limit", its scaling should be in between the scalings (4) and (5). With this uncertainty, averaging over (4) and (5) and approximating the ratio of the decay lengths to one, we obtain:

$$n_e \sim \frac{B^{4/3}}{q^{11/6\pm1/6}R}\lambda_p^{2/3}f(s)^{5/6\pm1/6} \times \left(\frac{T_e}{T_e+T_i}\right)^{5/6\pm1/6}\frac{m_i^{1/12\pm1/12}}{Z_{eff}^{1/3}} \qquad (6)$$

Note that the region in the (n_e,T_e) space bounded by the ideal ballooning curve, route 3 and the L-H transition threshold, is not accessible for the plasma as being above the threshold for type III ELMs.

Finally, we can identify one additional operational point which can be described by the scaling following from fixing parameters (2) and (3). This point should be on the L-H transition curve at the density where it bends (near the point where the route 1 touches the L-H transition curve on Figure 3). It corresponds to the transition from the collisionless to collisional plasma in the sense that collisionless skin-depth (at lower densities where the L-H transition is essentially the condition on β, as was pointed out in the previous section) is replaced by the collisional skin-depth (at higher densities where the L-H transition is, for constant decay length $L_\perp$, essentially the condition on the critical electron temperature). Although this operational point corresponds to rather low densities and is not of a particular interest for our analysis in this paper, it is worth mentioning that the density scaling obtained by fixing parameters (2) and (3):

$n_e \sim \dfrac{B^{4/3}}{qR}L_\perp^{2/3} \times \dfrac{1}{Z_{eff}^{1/3}m_i^{1/3}}$, is again rather close to scalings (4) and (5).

6. INFLUENCE OF q ON THE H-MODE OPERATION RANGE AT HIGH DENSITIES

The changes in the operational space for an ELMy H-mode plasma in the n_e - T_e diagram caused by varying safety factor q are schematically illustrated in Figure 5. In this figure we show the case where the variation in q is achieved by varying the plasma current, while the magnetic field is kept constant. In this instance, the L-H transition boundary is the same for low and high q plasmas. In the other case (fixed plasma current I_p, varying B, not shown in the figure) the ideal ballooning limit is fixed, and the changes in the operational space are due to the scaling of the L-H critical temperature ($T_e \sim B^{2/3}$). Due to the strong dependence of the ideal ballooning limit on q, the density corresponding to the transition between type I and type III ELMs is higher for the low q discharge, in accordance with Eq. (4). The separation between the ideal ballooning limit curve and the L-H transition boundary, however, is also increased since the latter does not depend on q. It is therefore not clear, *a priori*, how the temperature corresponding to the type I - type III transition should react with changing q.

The scaling for the edge temperature at the type I to III ELM transition is obtained by eliminating the density from the similarity parameters (1) and (2), yielding:

$$(T_e + T_i)T_e^2 \sim \frac{B^2}{q}\lambda_p Z_{eff} \tag{7}$$

We note that the critical temperature, similarly to the critical density defined in (4), depends both on B and q. At constant B, the critical edge temperature for the type I to III transition
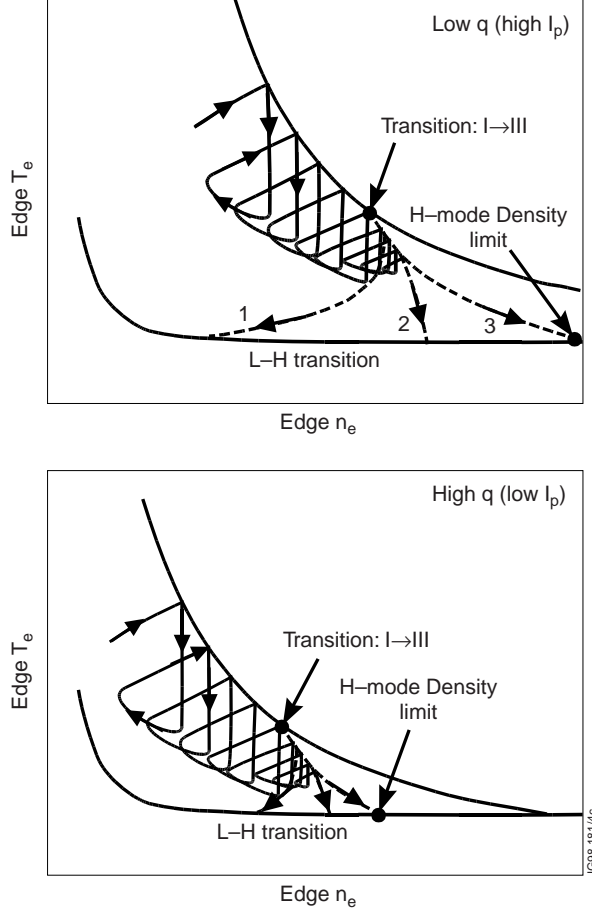

Figure 5: Schematic illustration of the influence of the safety factor q on the H-mode operational range, in the case of fixed toroidal field B.

increases at low q, consistently with the increase in the critical density, since this transition point is also by definition at the ideal ballooning limit. Experimental evidence from JET confirms that the critical temperature for the transition increases with increasing q at constant plasma current (and corresponding the critical density is lower) [23].

As for the L-H transition threshold, the scaling for the electron temperature follows from the similarity parameter (3):

$$T_e^3 \sim B^2 L_\perp Z_{eff} / \sqrt{m_i} \tag{8}$$

11

which is very similar to Eq. (7) except for the absence of the q-dependence. The temperature gap between the transition from type I to type III ELMs and the L-H transition threshold should therefore be wider for low q discharges allowing more margin for operating with type III ELMs while maintaining good confinement (provided that $L_\perp$ and λ_p behave in the same way).

7. MORE DETAILED SCALINGS FOR THE TYPE I - TYPE III ELM TRANSITION POINT

The "H-mode density limit" point as defined in Section 5 is not likely to be an acceptable operating point for a reactor, due to the poor energy confinement (ITER requires H_{93}~0.85 for ignition). The compatibility of any particular operational point identified by our analysis with the confinement requirements of a reactor can be assessed precisely only by comparison with experiments. Nonetheless, the point on the operational n_e - T_e diagram corresponding to the type I - type III ELM transition is of particular interest, since it may provide both reasonable confinement and benign ELMs (i.e. acceptable power load onto the divertor target). However, to make more detailed predictions for ITER, the dimensional approach has to be extended to include expressions for the edge transport coefficients, in order to replace the unknown dependence of the pressure decay length λ_p present in Eqs. (4) and (6).

The scaling for the density corresponding to this operational point is given by Eq. (4) that was derived by fixing parameters (1) and (2): $q^2 R \nabla \beta / f(s)$ (ideal ballooning limit) and $Z_{eff} n_e q R / T_e^2$ (collisionality). The above scaling could be used, for example, to simulate ELMy H-modes in ITER, taking JET as a model once the edge collisionality of a particular ITER regime is known. In addition, fixing q would ensure an improved simulation of ITER regimes since another important similarity parameter, (3): $T_e^3 / (B^2 L_\perp Z_{eff} / \sqrt{m_i})$, which accounts for micro-turbulence and defines the position of the L-H transition boundary, would be automatically matched very closely, as follows from the close similarity between scalings (4) and (5). These arguments provide strong motivation to elaborate further and consider the various possible scalings for the pressure decay length λ_p.

Most of the transport models give expressions for the electron heat conductivity χ_e which can subsequently be used to derive scalings for the temperature decay length λ_{T_e} at the separatrix, by assuming parallel heat conduction to the target. This decay length represents only one component of the pressure decay length λ_p, with the two remaining components being the density decay length λ_n and the ion temperature decay length λ_{T_i}. Ideally, λ_n and λ_{T_i} should also be derived from particle and heat balance equations, which include sources due to micro-turbulence, sinks to the target and sinks/sources due to plasma-neutral interaction (for λ_{T_i} and λ_n respectively). However, our knowledge of edge transport does not allow us to carry out such a

detailed analysis, therefore we make the reasonable assumption that λ_p should scale similarly to λ_{T_e}. This assumption is substantiated below.

Owing to $1/\lambda_p = 1/\lambda_n + 1/\lambda_{(T_e+T_i)}$, the total pressure decay length λ_p is smaller than the decay length for the sum of ion and electron temperatures: $\lambda_p < \lambda_{(T_e+T_i)}$. The latter, in turn, should be greater than the electron temperature decay length alone: $\lambda_{(T_e+T_i)} > \lambda_{T_e}$, due to the large electron heat sink to the target which sharpens the T_e gradient. Therefore, the combination of the two relationships $\lambda_p < \lambda_{(T_e+T_i)}$ and $\lambda_{T_i} > \lambda_{T_e}$ (note that also the density decays) supports our simplified hypothesis that the two decay lengths, λ_p and λ_{T_e} should not be too dissimilar. Moreover, by taking into account that $1/\lambda_{p_e} = 1/\lambda_n + 1/\lambda_{T_e}$, it is easy to show that both decay lengths should be within the same margins: $\lambda_{p_e} < (\lambda_{T_e}, \lambda_p) < \lambda_{(T_e+T_i)}$.

The above considerations give some more confidence in the assumption that λ_p and λ_{T_e} should have similar scalings. Lastly, we argue that any small deviations between the scalings for λ_p and λ_{T_e} should not generate large errors in the predictions for the density scaling (4), since the dependence of n_e on the pressure decay length is weakened by the 2/3 power. In the rest of this paragraph, we will analyse several transport models for χ_e or directly for λ_p, and derive explicit scalings for the critical density at the transition from type I to III ELMs.

The first model to be considered for χ_e is the one which is consistent with the assumption that micro-turbulence is controlled by the parameter (3), that corresponds to the collisional skin-depth scaling: $\chi_e \sim Z_{eff} T_e^{-3/2}$. It has been shown that this model fits well experimental data from probe measurements on JET and Alcator C-Mod (see [31], but with the correction for the contribution of Z_{eff}, omitted in this Reference but now included). This scaling follows directly from the definition of the collisional skin-depth: $\Delta_{skin} = c/\sqrt{4\pi\sigma\nu}$ (where $\sigma \sim T_e^{3/2}/Z_{eff}$ - Spitzer conductivity and ν - frequency of fluctuations), and an estimate of the mixing length for transport coefficients: $D_\perp, \chi \sim \Delta_{skin}^2 \times \nu$.

The electron heat balance equation, which includes parallel heat conduction to the target, gives the following expression for λ_{T_e}:

$$\lambda_{T_e} \sim qR\sqrt{Z_{eff} n_e \chi_e}/T_e^{5/4} \tag{9}$$

which will be used as the scaling for λ_p. The scaling for the critical density (assuming for simplicity $T_e \sim T_i$) can then be derived from the following system of equations:

$$n_e \sim \frac{B^{4/3}}{q^{5/3}R}\frac{\lambda_p^{2/3}f(s)^{2/3}}{Z_{eff}^{1/3}}, \quad \lambda_{T_e} \sim \frac{qR\sqrt{Z_{eff}n_e\chi_e}}{T_e^{5/4}}, \quad T_e^2 \sim Z_{eff}n_e qR \tag{10}$$

Finally, using the expression for χ_e given by the collisional skin-depth model, we obtain:

$$n_{e,crit} \sim \frac{B}{q^{5/4}R^{3/4}} \frac{f(s)^{1/2}}{Z_{eff}^{1/4}} \tag{11}$$

In order to assess the sensitivity of the scaling for the critical density $n_{e,crit}$ on the assumptions made about the dependence for χ_e, a number of other scalings for heat conduction have been considered. In particular, we have used the results of the comparison of theoretical models for scrape-off layer widths with data from COMPASS-D, JET and Alcator C-Mod contained in the paper by Connor et al. [32]. The four models which were found to be in the best agreement with the electron heat conduction extracted from the experiments are listed in the first row of Table 1. Apart from the already used "drift wave with collisional skin-depth" model (model I, according to the nomenclature adopted in [32]), these models are: "collisionless skin-depth" (O), which gives the same results as "collisionless MHD interchange near β_{crit}" (D), "charge-exchange collisions": $D_\perp \sim \nu_{cx}\lambda_{cx}^2 \sim \sqrt{T}/n_e$ (M) and "drift wave with collisionless skin-depth" (J). In addition, four other popular scalings for χ_e and the pedestal width are considered in the second row of Table 1: Bohm scaling, λ_p proportional to ion poloidal Larmor radius $\rho_{s\theta}$ (suggested by Parail for the pedestal width scaling, $\Delta \sim \rho_{s\theta}$, in [33]), and $\lambda_p \sim \sqrt{a\rho_{s\theta}}$, (suggested by Lingertat for the pedestal width scaling, $\Delta \sim \sqrt{a\rho_s}$, in [17]) and, finally, the constant χ_e scaling.

model	drift wave with collisional skin-depth: $\chi_e \sim Z_{eff}/T_e^{3/2}$	collisionless skin-depth: $\chi_e \sim \sqrt{T_e}/n_e qR$	drift wave with collisionless skin-depth: $\chi_e \sim \sqrt{T_e}/n_e\lambda_n$	charge-exchange collisions: $\chi_e \sim D_\perp \sim \dfrac{\sqrt{T}}{n_e}$
scaling for n_e	$\dfrac{Bf(s)^{1/2}}{q^{5/4}R^{3/4}Z_{eff}^{1/4}}$	$\dfrac{B^{4/5}f(s)^{1/2}}{q^{6/5}R^{4/5}Z_{eff}^{2/5}}$	$\dfrac{B^{12/11}f(s)^{6/11}}{q^{13/11}R^{7/11}Z_{eff}^{3/11}}$	$\dfrac{Bf(s)^{1/2}}{qR^{1/2}Z_{eff}^{1/4}}$
model	Bohm diffusion: $\chi_e \sim T_e/B$	as for pedestal width [33]: $\lambda_p \sim \rho_{s\theta}$	as for pedestal width [17] $\lambda_p \sim \sqrt{a\rho_{s\theta}}$	constant conductivity: $\chi_e = const$
scaling for n_e	$\dfrac{B^{12/11}f(s)^{8/11}}{q^{15/11}R^{7/11}Z_{eff}^{3/11}}$	$\dfrac{B^{4/5}f(s)^{4/7}}{qRZ_{eff}^{1/5}}$	$\dfrac{B^{12/11}f(s)^{8/11}}{q^{15/11}R^{7/11}Z_{eff}^{3/11}}$	$\dfrac{B^{16/13}f(s)^{8/13}}{q^{17/13}R^{12/13}Z_{eff}^{5/13}}$

Table 1: Scalings for the critical edge density for the type I - type III ELM transition, corresponding to different transport models for χ_e and λ_p

All but one of the models analysed yielded density scalings for the type I - type III ELM transition close to the Greenwald-Hugill scalings (for constant plasma elongation in case of the Greenwald scaling): $n_e \sim B^\alpha / q^\beta R^\gamma$ with coefficients α, β and γ close to unity. The exception is the charge-exchange collisions model which gives a very weak scaling against major radius ($R^{-1/2}$). Therefore, we tend to ignore the results of this model as unrealistic. Also, despite the fact that this model performed well in the statistical analysis of the scrape-off layer widths in [32], we are of the view that the charge-exchange collisions are very unlikely to be the dominant effect in the plasma transport. The remaining models predict:

- α close to unity, in agreement with the Greenwald-Hugill dependence (the constant conductivity model shows the strongest deviation from the linear dependence on B with α=16/13).

- β>1 (except for the $\lambda_p \sim \rho_{s\theta}$ model which yields β=1).

- γ<1 (again except for the $\lambda_p \sim \rho_{s\theta}$ model which yields γ=1).

8. COMPARISON OF PREDICTIONS WITH JET EXPERIMENTAL DATA

As it was highlighted in Section 2, stronger than the inverse linear dependence on q for the H-mode density limit was observed in ASDEX, in agreement with our model. To verify the predictions of the model in JET, in particular for the type I to type III ELM transition point, a dedicated series of discharges with varying q have been carried out. For this particular experiment, the shape of the plasma (hence, the edge shear) was fixed, as well as the divertor geometry (separatrix on the horizontal divertor plates) and the additional heating (NB injection of 14 MW). The value of q was varied from 2.5 to 4.7. To test independently the effect of the variation of the plasma current and of the toroidal field, the q scan was carried out twice, first at fixed B and then at fixed I_p. Each discharge was repeated with increasing gas fuelling. The results of this experiment (reported in detail in [23]) are in very good agreement with our model. In particular, we have verified the q-dependence of the scaling for the critical density for the transition from type I to type III ELMs, Eq.(11), against the experimental data. This is shown in Figure 6, where the line average density at the transition versus the scaling parameter $B/q^{5/4}$ is plotted (R, Z_{eff} and the shear are the same for all the discharges). Note that the use of the line average density for the scaling implies a fixed proportionality between the core and the edge density at the type I to III ELM transition. The good agreement between the experiment and the prediction give one confidence on the validity of the assumption for our modelling of the high density ELMy H-modes. The analysis of the JET data alone does not allow us to check the major radius dependence of the critical density in equation (11).
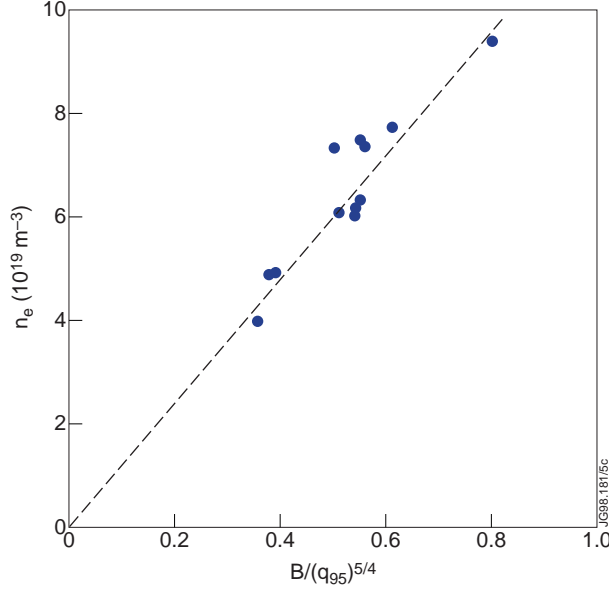
15

Figure 6: Core line average density versus the critical density scaling corresponding to the type I - type III ELM transition (at fixed shear, R and Z_{eff}) for a series of JET high density ELMy H-modes. The details of the experiment are described in the main text.

9. CONCLUSIONS

High density H-mode plasmas in different tokamaks show strong similarities with respect to the confinement properties, maximum density, ELM behaviour etc. In all machines, the highest density achievable while maintaining H-mode confinement is found to scale approximately as $\bar{n}_e \sim B/qR$, in agreement with the Greenwald-Hugill scaling. Developing our previous studies which highlight the role of confinement degradation at the plasma edge in the H-mode density limit [4], we have selected some specific mechanisms which, in our view, are likely to be the dominant transport mechanisms at the plasma edge. By fixing two out of the three dimensionless parameters (similarity parameters) which reflect the strength of these mechanisms, we were able to find the relationships between physical parameters corresponding to some characteristic operational points.

The main assumptions of our model have been outlined theoretically and partly already confirmed by experimental results. We assumed that: a) type I ELMs are triggered when the edge pressure gradient reaches the ideal ballooning limit, b) collisionality is the critical parameter for the onset of type III ELMs, which are likely to be caused by resistive ballooning instabilities, and c) we use the form of the L-H transition threshold (from [29]) which, in accordance with experimental evidence, gives a formulation for the threshold mainly in terms of the edge electron temperature and the toroidal field.

Fixing the selected similarity parameters allowed us to understand features of the H-mode operational space as seen in the edge n_e-T_e diagram. The scalings for the highest densities

16

achievable and the operational point corresponding to the type I - type III ELM transition were found to be in reasonable agreement with experimental findings. They roughly follow the Greenwald-Hugill scaling $\bar{n}_e \sim B^\alpha / q^\beta R^\gamma$ with α, β and γ close to unity. However, the q-dependence was found to be stronger than in this scaling ($\beta > 1$) in agreement with data from ASDEX and the results of a series of dedicated experiments in JET. The expected R-dependence is, on the contrary, weaker than inverse linear ($\gamma < 1$). It is important to note that the combination of any two out of the three similarity parameters yielded density scalings close to the Greenwald-Hugill scalings, indicating that the scalings for the main points on the n_e-T_e operational diagram are very close to each other and that the shape of this diagram is relatively independent of the machine/regime parameters. It should therefore be easily transferable from one machine to another to allow for a multi-machine scaling.

One particular scaling derived for the critical density at the extreme edge (close to the separatrix) for the type I - type III ELM transition point, corresponding to the collisional skin-depth model for χ_e in the scrape-off layer: $n_{e,crit} \sim \dfrac{B}{q^{5/4} R^{3/4}} \dfrac{f(s)^{1/2}}{Z_{eff}^{1/4}}$, was found to be in a good agreement with the experimentally obtained dependence of the line averaged density $\bar{n}_e$ on $B / q^{5/4}$ in JET. The scaling for $n_{e,crit}$, however, was found to be not very sensitive to the transport model selected and other models yielded similar dependencies. We attribute a good correspondence between our scaling for the extreme edge density $n_{e,crit}$ and the experimentally measured line averaged density to the fact that the ratio $n_{e,crit} / \bar{n}_e$ in high density ELMy H-modes is rather high and is likely to be constant. The exact location of the position inside the separatrix (or at the separatrix) where the derived scalings should be applied still remains an open question, but we suspect that the role of the extreme edge, very close to the separatrix, could be crucial. Further experimental evidence is needed to clarify this outstanding issue.

ACKNOWLEDGEMENTS

REFERENCES

[1]   Wagner F, Becker G, Behringer K et al 1982 Phys. Rev. Lett. **49** 1408
[2]   Aymar R, Chuyanov V, Huguet M et al. And the ITER Joint Central Team and Home Teams, IAEA-CN-64/O41-1, Fusion Energy 1996, Vol 1, p 3
[3]   ITER Confinement Database and Modelling Working Group 1997 Plasma Phys Control Fusion **39** B115

[4]   Saibene G, Balet B, Clement S et al 1997 Proc. 24th Eur. Conf. on Control. Fusion and Plasma Phys. (Berchtesgaden 1997) (Geneva: European Physical Society) Vol 21A, part I, p 49

[5]   Horton L D and the JET Team to be published in Nucl. Fusion

[6]   Mertens V, Herrmann A, Kallenbach A et al, "Edge and Divertor Physics in ASDEX Upgrade with Emphasis on Density Limit Characteristics", IAEA-CN-64/A4-4, Fusion Energy 1996, Vol 1, p 413

[7]   Suttrop W, Kaufmann M, de Blank H J et al 1997 Plasma Phys. Control. Fusion **39** 2051

[8]   Maingi R, Mahdavi M A, Jernigan T C et al 1997 Phys. Plasma **4** 1752

[9]   Kamada Y, Yoshino R, Ushigusa K et al IAEA-CN-64/A1-6, Fusion Energy 1996, Vol , p 247

[10]   Zohm H 1996 Plasma Phys. Control. Fusion **38** 105

[11]   Hill D N 1997 J. Nucl. Mater. **241-243** 182

[12]   Connor J W 1998 Plasma Phys. Control. Fusion **40** 191

[13]   Gauthier E, Chankin A, Clement S, Coad P, Davies S, Fishpool G, Lingertat J and Matthews G 1997 Proc. 24th Eur. Conf. on Control. Fusion and Plasma Phys. (Berchtesgaden 1997) (Geneva: European Physical Society) Vol 21A, part I, p 61

[14]   Greenwald M, Terry J L, Wolfe S M, Ejima S, Bell M G, Kaye S M and Neilson G H 1988 Nucl. Fusion **28** 2199

[15]   Stott P E, Hugill J, Fielding S J, McCracken G M, Powell B A and Prentice R 1979 Contr. Fusion and Plasma Phys. (Proc. 8th Euro. Conf. Prague, 1979) Vol 1 (Geneva: European Physical Society) p 151

[16]   Monk R D, Loarte A, Davies J D et al 1997 Proc. 24th Eur. Conf. on Control. Fusion and Plasma Phys. (Berchtesgaden 1997) (Geneva: European Physical Society) Vol 21A, part I, p 117

[17]   The JET Team (presented by M Keilhacker) 1997 Plasma Phys. Control. Fusion **39** B1

[18]   The JET Team (presented by C G Vlases) IAEA-CN-64/A1-4, Fusion Energy 1996, Vol 1, p 371

[19]   The JET Team (presented by D Stork) IAEA-CN-64/A1-1, Fusion Energy 1996, Vol 1, p 189

[20]   Borrass K, Lingertat J and Schneider R 1998 Contrib. Plasma Phys. **38** 130

[21]   Borrass K 1991 Nucl. Fusion **31** 1035

[22]   Post D, Stabler A and Neuhauser J 1997, "High Density ASDEX Discharges", ITER Memo G 18 MD 2 97-03-03 W 0.1 (Garching Joint Working Site)

[23]   Saibene G, Chankin A V, Balet B et al, "High Density ELMy H-Mode Studies at JET in ITER Relevant Scenarios", to be presented at the 1998 EPS ????????

[24]   Breger P, Flewin C, Zastrow K-D et al 1998 Plasma Phys. Control. Fusion **40** 347.

[25]   Huysman G T A, Hender T C, Alpert B 1998 Nucl Fusion **38** 179

18

[26] Kass T, Gunter S, Maraschek M et al 1998 Nucl. Fusion **38** 111

[27] Loarte A, Asakura N, Bosch H et al 1998 Contrib. Plasma Phys. **38** 11

[28] Righi E and the H-mode Database Working Group 1998, "Scaling of the H-mode Power Threshold for ITER", to be published in Plasma Phys. and Controlled Fusion

[29] Chankin A V and Matthews G F 1998 Contrib. Plasma Phys. **38** 177

[30] Chankin A V 1977 Plasma Phys. Control. Fusion **39** 1059

[31] Erents S K, LaBombard B, Chankin A V, Davies S J, Monk R D, Matthews G F and Stangeby P C Proc. 24th Eur. Conf. on Control. Fusion and Plasma Phys. (Berchtesgaden 1997) (Geneva: European Physical Society) Vol 21A, part I, p 121

[32] Connor J W, Counsell G, Erents S K, Fielding S J, LaBombard B and Morel K 1998, "Comparison of Theoretical Models for Scrape-Off Layer Widths with Data from COM-PASS-D, JET and Alcator C-MOD", UKAEA Fusion preprint 1998, UKAEA FUS 396, submitted to Nucl. Fusion

[33] Bak P, Balet B, Cherubini A et al 1996 Nucl. Fusion **36** 321